J. Membrane Biol. 57, 179–193 (1980)

The Journal of
Membrane Biology

The Cole-Moore Effect in Nodal Membrane of the Frog *Rana Ridibunda*: Evidence for Fast and Slow Potassium Channels

V.I. Ilyin, Irene E. Katina, A.V. Lonskii*, V.S. Makovsky, and E.V. Polishchuk**

Institute of Physiology, Leningrad University, Leningrad, 199164 USSR, Leningrad Nuclear Physics Institute, Academy of Science USSR, Gatchina, Leningrad District, 188350 USSR, and Institute of Cytology, Academy Science USSR, Leningrad, 190121 USSR

Summary. The K conductance (g_K) kinetics were studied in voltage-clamped frog nodes (*Rana ridibunda*) in double-pulse experiments. The Cole-Moore translation for $g_K - t$ curves associated with different initial potentials (E) was only observed with a small percentage of fibers. The absence of the translation was found to be caused by the involvement of an additional, slow, g_K component. This component cannot be attributed to a multiple-state performance of the K channel. It can only be accounted for by a separate, slow K channel, the fast channel being the same as the n^4 K channel in *R. pipiens*.

The slow K channel is characterized by weaker sensitivity to TEA, smaller density, weaker potential (E) dependence, and somewhat more negative E range of activation than the fast K channel. According to characteristics of the slow K system, three types of fibers were found. In Type I fibers (most numerous) the slow K channel behaves as an n^4 HH channel. In Type II fibers (the second largest group found) the slow K channel obeys the HH kinetics within a certain E range only; beyond this range the exponential decline of the slow g_K component is preceded by an E-dependent delay, its kinetics after the delay being the same as those in Type I fibers. In Type III fibers (rare) the slow K channel is lacking, and it is only in these fibers that the Cole-Moore translation of the measured $g_K - t$ curves can be observed directly.

The physiological role of the fast and slow K channel in amphibian nerves is briefly discussed.

Key words: Ranvier node, potassium currents, Hodgkin-Huxley kinetics, potassium channel conductance states.

Quantitative descriptions of the K conductance (g_K) kinetics in the node of Ranvier in terms of the Hodgkin-Huxley (HH) model (Hodgkin & Huxley, 1952) were given by Dodge (1963) and Frankenhaeuser (1963) for two different amphibian species. Dodge found no marked departure from the HH formalism in the frog *Rana pipiens*, while Frankenhaeuser was compelled to conclude that for the toad *Xenopus laevis* this formalism "is incomplete and, strictly considered, it is not correct."

Recently, in two other cases studied in detail, *R. ridibunda* and *R. esculenta*, it has been established that the g_K kinetics behave like those in *X. laevis* (*see* references below). No explanation for this strange difference between *R. pipiens* and other amphibian species has so far been offered. Meanwhile the answer to the question as to why the g_K kinetics in some (and probably most) amphibian nodes differ from the HH formalism may lead to a better understanding of the K channel performance.

Within the HH framework the K channel conductance is controlled by a number (x) of identical gating subunits, each of which can be only in one of two states, either closed (n_c) or open (n_o), the open-closed transition obeying the first-order kinetics:

$$n_c \underset{b_n}{\overset{a_n}{\rightleftharpoons}} n_o \tag{1}$$

$$\frac{dn}{dt} = a_n(1-n) - b_n \cdot n \tag{2}$$

where a_n and b_n are rate constants dependent on the membrane potential (E) but not on time (t). Following a step change in E from an initial value, E_1, to a final value, E_2, the relaxation of a gating subunit from an equilibrium state at E_1, $n_\infty(E_1)$, to a new equilibrium state at E_2, $n_\infty(E_2)$, will proceed as

$$n(t) = n_\infty(E_2) - [n_\infty(E_2) - n_\infty(E_1)] \exp(-t/\tau_n) \tag{3}$$

* *Address for reprint requests:* Institute of Physiology, Leningrad University, Leningrad, 199164 USSR.
** *Address for reprint requests:* Institute of Cytology, Academy of Science USSR, Leningrad, 190121 USSR.

0022-2631/80/0057-0179 $03.00

where $n_\infty = a_n(a_n+b_n)^{-1}$ and $\tau_n = (a_n+b_n)^{-1}$. As with the rate constants a_n and b_n, the relaxation time τ_n is determined by E_2 only: at a given test potential E_2 it should be the same, whatever the prepulse E_1 was. The gate (and the K channel) is open only when all x subunits are in the state n_o. The overall g_K of a K channel population can then be described as

$$g_K(t) = \bar{g}_K n^x(t) \tag{4}$$

where $\bar{g}_K$ is the maximum g_K.

The HH formalism for g_K kinetics is thus based on the single first-order variable n, and this fact allows a ready testing of the validity of this formalism. Indeed, Eq. (3) for n can be rewritten as

$$n(t) = n_\infty(E_2)\,[1-\exp(-(t-\Delta t)/\tau_n)] \tag{5}$$

for depolarizing E steps, when $E_1 < E_2$ and $n_\infty(E_2) < n_\infty(E_1)$, with

$$\Delta t = \tau_n \cdot \ln \frac{n_\infty(E_2)}{n_\infty(E_2)-n_\infty(E_1)} \tag{6}$$

and

$$n(t) = n_\infty(E_2)\,[1+\exp(-(t+\Delta t)/\tau_n)] \tag{7}$$

for repolarizing E steps, when $E_1 > E_2$ and $n_\infty(E_1) > n_\infty(E_2)$, with

$$\Delta t = \tau_n \cdot \ln \frac{n_\infty(E_2)}{n_\infty(E_1)-n_\infty(E_2)}. \tag{8}$$

Thus changing of initial conditions (prepulse E_1) should lead to parallel shift of the $n-t$ curve and, consequently, of the g_K-t curve along the t-axis if the test pulse E_2 remains constant. Therefore in the HH formalism the g_K kinetics should not depend on initial conditions, i.e., on the parameters of E_1. Hill and Chen (1972) and Chen (1976) extended the single-conductance HH model to multiple-conductance models, k-models. Since k-models are formally the same as in HH, the Cole-Moore translation should take place in these models as well.

Cole and Moore (1960) experimentally confirmed the translation in squid axon membrane. Dodge (1963) came to the same conclusion with *R. pipiens*, and this seems to be, so far, the only known example of the kind for amphibian myelinated fibers. In *X. laevis* both b_n (Frankenhaeuser, 1963) and a_n (*see* Makovsky (1975) for analysis of Frankenhaeuser's (1962) data) depend on prepulse duration. The dependence of g_K on initial conditions has also been reported for *R. ridibunda* in our preliminary publications (Ilyin et al., 1973, 1974*a*, *b*, 1977) and *R. esculenta* (Palti, Ganot & Stämpfli, 1976; Ganot, Palti & Stämpfli, 1978).

In this paper we show that in *R. ridibunda* node the dependence of g_K kinetics on the prepulse amplitude at repolarizations is the result of activation of two uncoupled g_K components, a fast and a slow, and we present evidence that at depolarizations the components obey n^4 kinetics but with different time and voltage dependencies of the HH variables. We attribute the slow g_K component to a slow K channel of the HH type, the fast K channel being most probably the same as in *R. pipiens*.

Materials and Methods

Preparation

Single large (15–20 μm) fibers were dissected from the sciatic nerve of the frog *R. ridibunda*. No effort was made to distinguish, between motor and sensory fibers.

Experimental technique

The voltage-clamp method used has been described elsewhere (Lonskii, Ilyin & Malov, 1972). It had a great deal in common with that of Nonner (1969), the main distinctions being:

1. Large internodal resistances were achieved with air gaps of fixed widths.
2. The liquid pool on the recording side was carefully shielded, and the shield was connected to the output of a cathode follower with a coefficient of amplification 0.998. This made it possible to reduce the input capacity to about 0.015 pF and to clamp the membrane potential in less than 15 μsec to within 1–2%. Further details can be found in Lonskii et al., 1972.

Solutions

Composition of the solution used (adjusted to pH 7.4) is given in Table 1. The temperature of the solutions bathing the node was 15–18 °C.

Solution 1 was used to check the functional condition of the node. Solution 2 was used for liquid pools for fiber cut ends on both sides of the node.

K ion accumulation in the perinodal space during outwardly directed I_K (Dubois & Bergman, 1975) may lead to an appreciable difference between time courses of g_K and I_K (Adam, 1973; Adelman, Palti & Senft, 1973). Therefore, all the experiments intended to measure g_K-t curves for subsequent quantitative analysis were performed in high K solution 4. The further advantages of high K solution were large and faithful I_K currents associated with repolarizing steps (I_K tails). This fact was of paramount importance in the present study because the model proposed is mostly based on evidence obtained from quantitative analysis of I_K-t curves measured in various double-pulse repolarization experiments.

Experimental Procedure

Programs of pulses applied to a node are described in the text and figure legends. Successive runs of a program were spaced at 2 sec. In between the runs the node was held at resting potential (E_R) assumed to be −70 mV. Prepulse E_1 was preceded by a holding potential E_0 with an amplitude of about −100 mV and a duration

Table 1. Composition of solution around the node (mM)

Solution	KCl	NaCl	$CaCl_2$	Tris Cl	TTX	TEA
1	2.5	125.5	2.5	5.0	0	0
2	128	0	0	5.0	0	0
3	2.5	125.5	2.5	5.0	$3 \cdot 10^{-4}$	0
4	128	0	2.5	5.0	$3 \cdot 10^{-4}$	0
5	2.5	125.5	2.5	5.0	$3 \cdot 10^{-4}$	20
6	128	0	2.5	5.0	$3 \cdot 10^{-4}$	20

TTX: tetrodotoxin; TEA: tetraethylammonium bromide. In solution 2 KF was sometimes used instead of KCl.

of 100 msec (*see*, e.g., inset in Fig. 4). To determine the absolute membrane potential (E) of a node, the node was destroyed at the end of experiment by a strong positive pulses and the residual potential was subtracted from all the pulses of the programs used in this experiment. E is reported as inside minus outside potential.

Obtaining the net I_K

Each program of pulses was repeated twice: first in a working solution (3 or 4) and then in its counterpart solution (5 or 6, respectively) containing 20 mM TEA (*see* Table 1). "The potassium currents I_K" are the net currents obtained after subtraction of the currents in solutions 5 or 6 from the corresponding currents in solutions 3 or 4. By this procedure we excluded not only the currents of capacitative surge and ohmic leak but also the exponentially decaying current (Hille, 1967*b*), unaffected by TTX and TEA, observed in some fibers.

Analysis of I_K

The steady-state value of $I_K(I_{K_\infty})$ at repolarizations was measured at the end of a 100-msec test pulse. An exponential time sweep was used to show both the fast and slow portions of I_K on the same record. The photographic records of currents were digitized by an A/D converter PUOS (Russian index). The net $I_K - t$ curves were recalculated into linear time scale and analyzed either graphically or on a computer by fitting to the observations the modified HH Eq. (17) with the method of least squares. Minimization of variance was performed with the method of steepest descent. Special attention was given to test that a local minimum had not been mistaken for the absolute minimum being sought (Brent, 1973).

Results and Analysis

We shall first consider the results obtained in the repolarization experiments because they are important for an understanding of the depolarization data.

1. K Currents at Repolarization: Results

In all repolarization experiments the node under investigation was in high K solution 4. About 400 nodes were examined, and three basic types of I_K currents (tails) were identified. Each type is described under separate paragraphs. At present we cannot give the exact evaluation of the occurrence of each type because not all the material obtained was treated quantitatively and many I_K tails were classified by sight.

1.1. Type I Fibers. Such fibers were the most frequent. A typical case is presented at the top of Fig. 1: five I_K tails associated with five different prepulses E_1 and a constant test pulse E_2 are shown. It is seen that each

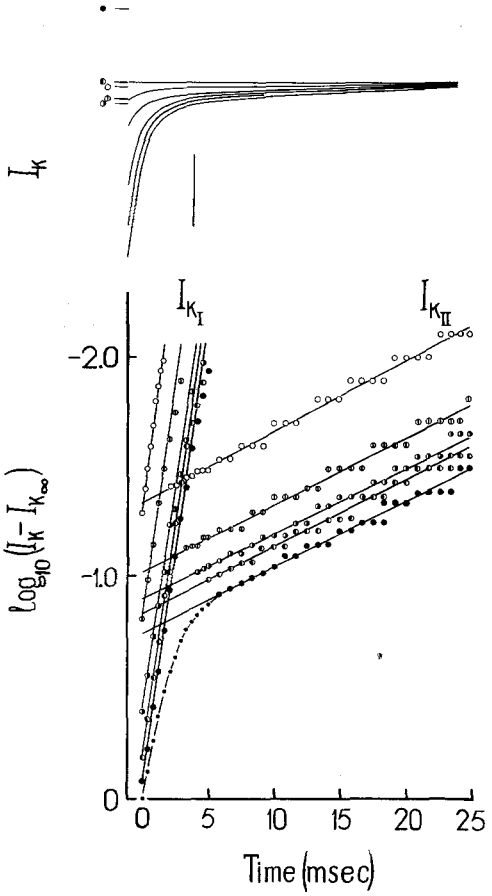

Fig. 1. The Cole-Moore test for repolarization in a Type I fiber. *Above:* I_K tails associated with E steps to $E_2 = -106$ mV from different E_1 (downwards from the base-line): -60, -48, -30, -1, $+55$ mV. I_K levels, immediately before a step, at these E_1 values are indicated by symbols ○, ◔, ◑, ◐, ●, respectively. Duration of E_1, 40 msec. (For other details, *see* text and inset in Fig. 4.) Note that the tails are nonparallel. 128 mM K Ringer plus $3 \cdot 10^{-4}$ mM TTX. Leakage current subtracted. Calibration current bar, $5 \cdot 10^{-9}$ A. Time axis as below. *Below:* graphical analysis of the I_K tails above. I_{K_∞}: I_K value at $t = 100$ msec. Only the largest $(I_K - I_{K_\infty})$ tail, associated with $E_1 = +55$ mV, is fully represented, by way of illustration, by the undermost dashed-dotted curve continued as solid curve. The maximum value of this tail (at $t = 0$) is normalized to 1. The other four $(I_K - I_{K_\infty})$ tails are only represented by their components I_{K_I} and $I_{K_{II}}$. Symbols relate to E_1 values before a step, as above. Note that $I_{K_I} - t$ and $I_{K_{II}} - t$ curves are parallel (within their families). For values of relaxation times τ_{K_I} and $\tau_{K_{II}}$, *see* Table 2 (columns 3 and 6, respectively). Node 371

tail consists of a fast and a slow portion. In accordance with Eqs. (7)-(8), the $I_K - t$ curves shift to the left along the t-axis with more negative E_1, but the shifts are nonparallel.

However, from graphical analysis at the bottom of Fig. 1 it is clear that each I_K tail can be divided into a fast (I_{K_I}) and a slow ($I_{K_{II}}$) component, which do shift in parallel along the t-axis and are the exponential functions of time. This means that their associated relaxation times τ_{K_I} and $\tau_{K_{II}}$ are independent of the prepulse amplitude, i.e., the behavior of each component is controlled by a first-order variable. In this experiment there were nine different values of E_1. The relaxation times obtained are collected in Table 2 (column 3 for τ_{K_I} and column 6 for $\tau_{K_{II}}$). For this node, at $E_2 = -106$ mV, τ_{K_I} was 0.95 ± 0.03 msec and $\tau_{K_{II}}$ was 14.2 ± 0.7 msec (mean $\pm$ SD for $n=9$). It should be noted that $\tau_{K_{II}}$ (as τ_{K_I}) is the same regardless the direction of I_K during prepulse. This means that $I_{K_{II}}$ cannot be due to washing out of excess K ions

Table 2. Time constants τ_{K_I}, $\tau_{K_{II}}$ and τ_K (for a node in Fig. 10) obtained from graphical analysis of tails of potassium currents associated with repolarizing steps from different conditioning potentials E_1 to the same test potential E_2

1	2	3	4	5	6	7	8
E_1 (mV)	τ_K (msec)	τ_{K_I} (msec)	τ_{K_I} (msec)	τ_{K_I} (msec)	$\tau_{K_{II}}$ (msec)	$\tau_{K_{II}}$ (msec)	$\tau_{K_{II}}$ (msec)
+65			1.05	1.04		22.2	21.7
+60	0.99						
+55		0.96			14.3		
+46			1.05	1.08		20.0	22.9
+42	0.99						
+36			1.03	1.00		23.8	19.5
+29		0.96			15.0		
+23	1.00						
+16			1.00	0.90		24.0	20.2
+10	1.02	0.95			14.8		
+4			1.03	1.01		20.7	22.7
+1	1.00						
−1		0.96			14.2		
−10			1.04	0.86		19.8	20.1
−14	1.00						
−19		0.94	1.05	1.03	13.1	22.6	21.6
−26	0.96		0.90	1.00		22.7	19.8
−30		0.98			14.9		
−35	1.00		1.00	1.05		20.8	20.3
−40		0.89			13.4		
−42	0.98		1.06	1.04		22.5	20.0
−48	0.99	0.97			14.2		
−53	1.00						
−60	1.01	0.96	1.05	1.03	13.5	20.5	20.4
Mean	0.995	0.95	1.02	1.00	14.2	21.7	20.8
±SD	±0.015	±0.03	±0.05	±0.07	±0.7	±1.5	±1.2

Column 2: node 518; E_1: 50 msec duration; E_2: −98 mV.
Column 3, 6: node 371; E_1: 40 msec duration; E_2: −106 mV.
Column 4, 7: node 253; E_1: 20 msec duration; E_2: −100 mV.
Column 5, 8: node 253; E_1: 500 msec duration; E_2: −100 mV.

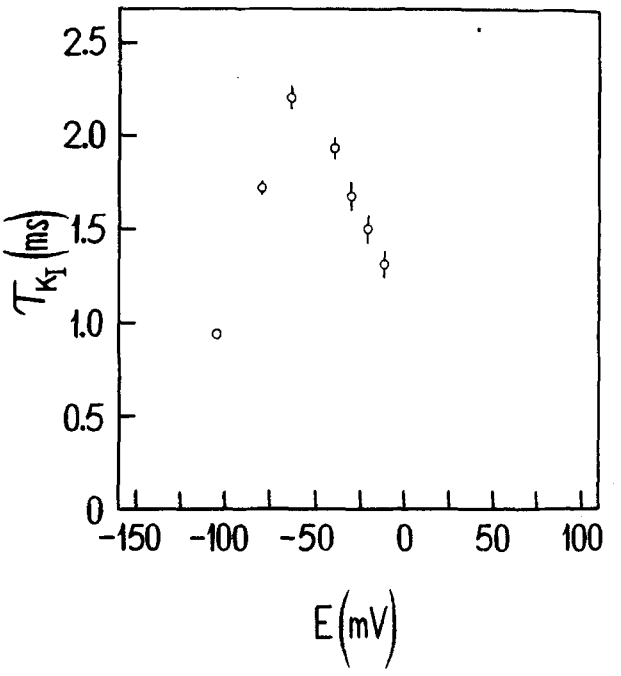

Fig. 2. The relationship $\tau_{K_I} - E$ measured with different prepulses E_1. E values on the abscissa are values of the test potential E_2 used; duration of E_1, 40 msec. Prepulses E_1 were:

for $E_2 = -106$ mV: −60, −48, −40, −30, −19, −10, −1, +10, +29, and +55 mV;
for $E_2 = -80$ mV: −48, −40, −30, −19, −10, −1, +10, +29, and +55 mV;
for $E_2 = -65$ mV: −30, −19, −10, −1, +10, +29, and +55 mV;
for $E_2 = -40$ mV: −19, −10, −1, +10, +29, and +55 mV;
for $E_2 = -30$ mV: −1, +10, +29, and +55 mV;
for $E_2 = -19$ mV: +10, +29, and +55 mV;
for $E_2 = -10$ mV: +10, +29, and +55 mV.

Bars indicate SD from the mean. For τ_{K_I} (−106 mV) SD is too small to be shown on the scale (0.95 ± 0.03 msec, *see* Table 2, column 3). The same experiment as in Fig. 1

accumulated in the perinodal space. Moreover, the high K solution we used to bathe the node ruled out the possibility of K ion accumulation (*see* Figs. 6 and 7).

A similar set of pulses was applied to this node six more times with six other test pulses E_2. The mean relaxation times obtained, with their SD, are shown in Fig. 2 (τ_{K_I}) and Fig. 3 ($\tau_{K_{II}}$). It is seen that the relaxation times do not depend on E_1 at any E_2. An increase in SD with E_2 in Figs. 2 and 3 must be attributed to progressively less accurate measurements of τ_{K_I} and $\tau_{K_{II}}$ as E_2 values increase due to smaller I_K tails and progressively lesser number of independent measurements (*see* legend to Fig. 2).

The other way to change initial conditions is to vary the prepulse duration. We only used long prepulses E_1. Some results are shown in Fig. 4. The

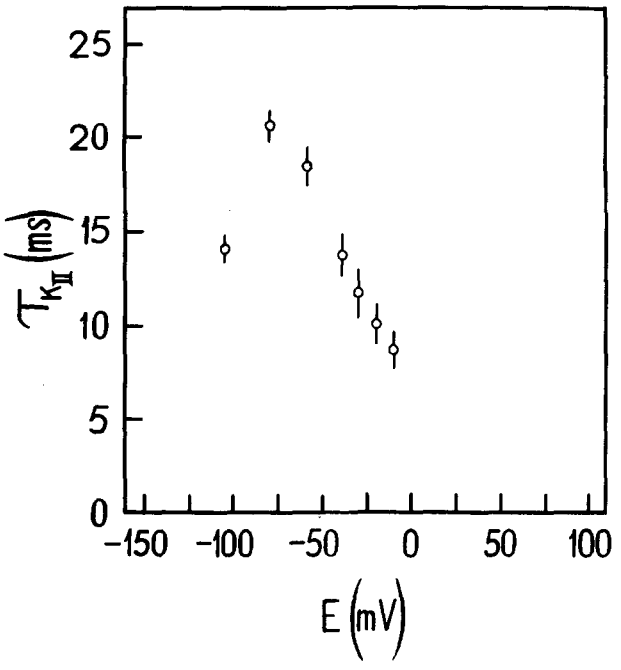

Fig. 3. The relationship $\tau_{K_{II}} - E$ measured with different prepulses E_1. All the details are as in Fig. 2. The experiment is the same as in Figs. 1 and 2

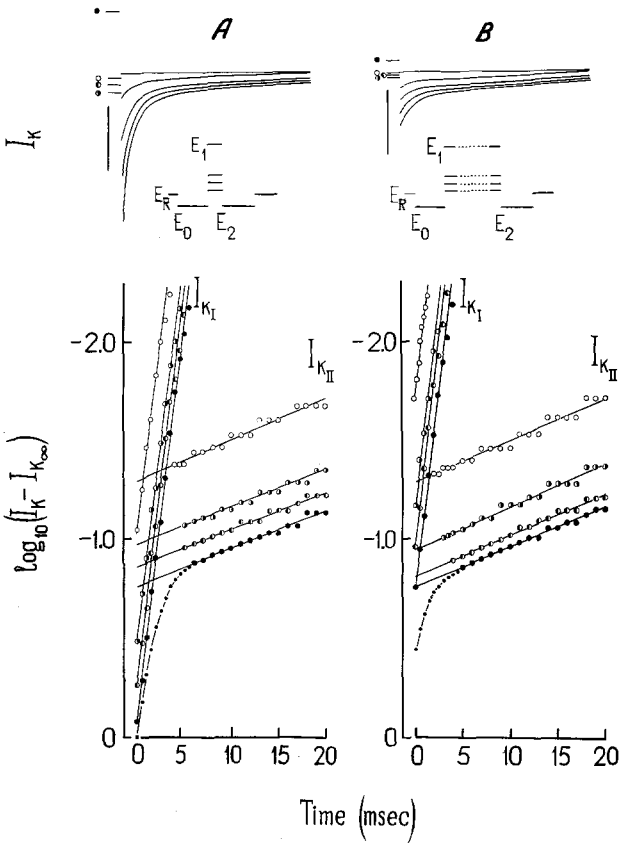

Fig. 4. The Cole-Moore test at repolarizations in a Type I fiber with prepulses of 20 msec (*A*) and 500 msec (*B*). *Above:* I_K tails associated with steps from E_1 (downwards from the base-line): −60, −42, −19, and +65 mV to $E_2 = -100$ mV. I_K levels immediately before a step at these E_1 values are indicated by symbols ○, ◑, ◐, and ●, respectively. *Inset:* the program of stimuli. (For other details, *see* text.) 128 mM K Ringer solution plus $3 \cdot 10^{-4}$ mM TTX. Leakage current subtracted. Calibration current bar, $5 \cdot 10^{-9}$ A. The time axis was as below. *Below:* graphical analysis of the I_K tails above. All the details are as in Fig. 1. Note that the sole effect of a long conditioning prepulse consists of a reduction of the magnitude of a fast current I_{K_I}. For values of time constants, *see* Table 2, columns 4 and 7 (short E_1) and columns 5 and 8 (long E_1). For relative values of amplitudes of instantaneous currents $I_{K_{I0}}$ and $I_{K_{II0}}$ on linear scale, *see* Fig. 5*A* and *B*, respectively. Node 253

program of E steps was here analogous to that in Fig. 1, but prepulses E_1 were 20 and 500 msec long. It seen again that I_K tails can be resolved into two components, I_{K_I} and $I_{K_{II}}$, which shift along the t-axis with changing of E_1 amplitude. The changing of E_1 duration results in a parallel shift of I_{K_I} and practically no shift of $I_{K_{II}}$. This means that I_{K_I} is and $I_{K_{II}}$ is not inactivated by long prepulses E_1 and that neither τ_{K_I} nor $\tau_{K_{II}}$ depend on prepulse duration (*see* Figs. 5–7 and Table 2).

Table 2 presents quantitative data illustrating independence of relaxation times of both components on prepulse duration. With E_1 at 20 msec, τ_{K_I} was 1.02 ± 0.05 msec (column 4), and with E_1 at 500 msec, it was 1.00 ± 0.07 msec column 5); $\tau_{K_{II}}$ values were, respectively, 21.7 ± 1.5 and 20.8 ± 1.2 msec (columns 7 and 8) (mean ± SD for $n = 11$).

In Fig. 5 the instantaneous amplitudes of I_{K_I} and $I_{K_{II}}$ from the above experiment are plotted against E_1. They are presented as $g_{K_{I\infty}}$ and $g_{K_{II\infty}}$ since, first, there being no K ion accumulation under these conditions (*see* Figs. 6 and 7), the time courses of g_K and I_K are the same and, second, there is every reason to believe that I_{K_I} is fully activated during E_1 of 20 msec duration (*see* Figs. 2 and 8*A*), and $I_{K_{II}}$ is fully activated during E_1 of 500 msec duration (*see* Figs. 3 and 8*B*). From Fig. 5 it can be seen that a long prepulse reduces g_{K_I} in this node to 0.2 of its initial value (Fig. 5*A*) but does not affect $g_{K_{II}}$ (Fig. 5*B*). A slight increase in $g_{K_{II\infty}}$ at large and negative prepulses in Fig. 5*B* may certainly be explained by the assumption that it takes longer than 20 msec to fully activate the slow component $g_{K_{II}}$ by negative potentials.

Figures 6 and 7 show another type of inactivation experiment. Full instantaneous values of I_K were measured here at different test potentials E_2 (Fig. 6) and divided into I_{K_I} and $I_{K_{II}}$ (Fig. 7; the procedure is described below). E_1 (67 mV) was at 50 and 500 msec. Again, during 500 msec $I_{K_{II}}$ did not change while I_{K_I} fell to 0.4 of its initial value. Figure 6 shows that E_K does not change during long polarization by a positive pulse as large as 67 mV. This means that the reduction of I_{K_I} in the above experiments is really

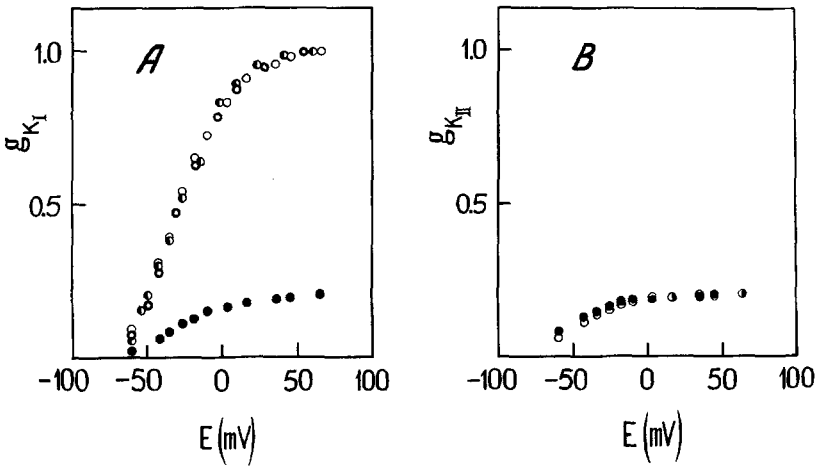

Fig. 5. Instantaneous conductances $g_{K_I}(A)$ and $g_{K_{II}}(B)$ measured at repolarization from values E_1 given by abscissa to $E_2 = -106$ mV (●), -100 mV (○, ●), -98 mV (◐). (*A*): g_{K_I} for: ●, node 371, E_1 40 msec (*see also* Fig. 1); ◐, node 518, E_1 50 msec (*see also* Fig. 10); ○, node 253, E_1 20 msec (*see also* Fig. 4*A*); ●, node 253, E_1 500 msec (*see also* Fig. 4*B*); (*B*): $g_{K_{II}}$ for: ○, node 253, E_1 20 msec (*see also* Fig. 4*A*); ●, node 253, E_1 500 msec (*see also* Fig. 4*B*). The maximum conductances g_{K_I} of all three nodes are normalized to 1. All other details as in Fig. 1, 4 and 10. Note that the plot in *A* reflects the potential dependence of the steady-state conductance g_{K_I}, $g_{K_{I\infty}}$, and in *B* the plot given by filled circles reflects the potential dependence of the steady-state conductance $g_{K_{II}}$, $g_{K_{II\infty}}$

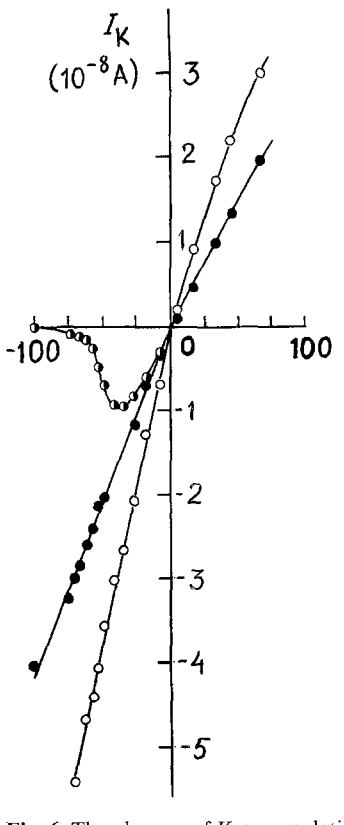

Fig. 6. The absence of K accumulation with isopotassium solution around the node. Amplitude of instantaneous currents I_{K_o} at repolarization to values E_2 given as E on the abscissa (for $E \leqq 5$ mV) from E_1 ($= +67$ mV) at 50 msec (open circles) and 500 msec (filled circles). The open and filled circles for $E > 5$ mV are for I_K values measured at the end of a depolarizing E_1 given as E on the abscissa. (Note that $E = E_2$ for $E \leqq 5$ mV and $E = E_1$ for $E > 5$ mV). The half-filled circles are for values of the same I_K tails at $t = 100$ msec, I_{K_∞}, (short E_1)

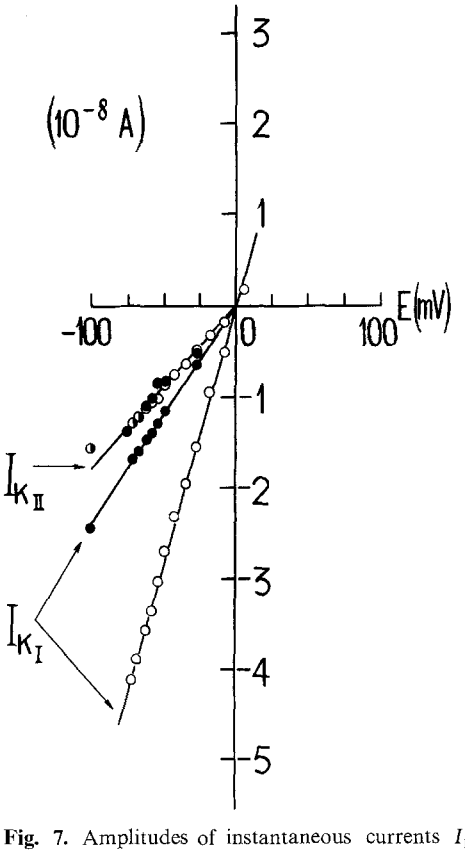

Fig. 7. Amplitudes of instantaneous currents $I_{K_{Io}}$ and $I_{K_{IIo}}$ at repolarization from $E_1 = +67$ mV to values E_2 given as E on the abscissa. (For details of construction, *see* text.) 128 mM KCl Ringer plus $3 \cdot 10^{-4}$ mM TTX. Node 508-2. The same experiment as in Fig. 6

due to inactivation; furthermore, the reduction of I_{K_I} occurs with constant E_{K_I} (Fig. 7).

The overall kinetics of I_K tails in Type I fibers can be expressed as

$$I_K(t)=I_{K_{I0}}\exp(-t/\tau_{K_I})+I_{K_{II0}}\exp(-t/\tau_{K_{II}})+I_{K_\infty} \quad (9)$$

where $I_{K_{I0}}$ and $I_{K_{II0}}$ are I_{K_I} and $I_{K_{II}}$ as in Figs. 1 and 4 at $t=0$, and I_{K_∞} is, as usual, I_K at $t=100$ msec. Now within the range of E_2 where I_{K_∞} values were negligibly small (*see* Fig. 6) the corresponding $I_{K_{I0}}-E_2$ and $I_{K_{II0}}-E_2$ characteristics were straight lines through $E_2=E_{K_I}=E_{K_{II}}=0$. But with those E_2 values where I_{K_∞} values were perceptibly large (*see* Fig. 6) (and it will be noted that $I_{K_{I0}}$ and $I_{K_{II0}}$ fall with increase in E_2) the same linear dependences took place only for plots $(I_{K_{I0}}+I_{K_{I\infty}})-E_2$ and $(I_{K_{II0}}+I_{K_{II\infty}})-E_2$, $I_{K_{I\infty}}+I_{K_{II\infty}}=I_{K_\infty}$ in Eq. (9). The values of $I_{K_{I\infty}}$ and $I_{K_{II\infty}}$ at corresponding E_2 were determined from $I_{K_{I0}}-E_1$ and $I_{K_{II0}}-E_1$ characteristics for this node, with $E_2=-100$ mV (i.e., with negligibly small I_{K_∞}), and E_1 duration 50 and 500 msec, respectively.

The relaxation times τ_{K_I} and $\tau_{K_{II}}$ of the components I_{K_I} and $I_{K_{II}}$ from the above experiment are shown in Fig. 8*A* and *B*, respectively. One can see that they do not depend on prepulse duration. One can also conclude that inactivation of I_{K_I} proceeds independently of its activation.

The behavior of an *i*-th component of g_K such as observed in the above experiments can be fully described with the use of two functions: $g_{K_{I\infty}}(E)$ and $\tau_{K_i}(E)$. However, in our experiments the concrete shapes of these functions markedly varied from fiber to fiber, especially those relating to the slow component $g_{K_{II}}$. Thus the relative value fo $\bar{g}_{K_{II}}$ with respect to the value of $\bar{g}_{K_I}$ ranged from 0.2 to 0.8 (being mostly between 0.2 and 0.3). The maximum values of $\tau_{K_{II}}$ were scattered within the range of 15–30 msec at 15–18 °C. The positions of $g_{K_{II\infty}}-E$ curves on the *E*-axis and their slopes also varied markedly, but these slopes were always considerably less steep than the slopes of $g_{K_{I\infty}}-E$ curves. As for the fast component g_{K_I}, the parameters characterizing its activation varied to a much lesser degree, the main source of variability being the degree of inactivation during the action of prepulse, which varied considerably from fiber to fiber (*cf.* Figs. 5*A* and 7). This inactivation corresponds to fast K inactivation described by Schwarz and Vogel (1971) in *X. laevis*. There is also a slow K inactivation in *R. ridibunda* nerves similar to that in *X. laevis* as described by Schwarz and Vogel, but we shall not deal with it here.

1.2. Type II fibers. This was the second largest group. Its distinctive feature is the behavior of the slow component $I_{K_{II}}$.

Figure 9 illustrates a typical case. Here E_2 was -104 mV and E_1 varied from 52 to -62 mV. It can be seen that I_K tails associated with $E_1=-62$ and

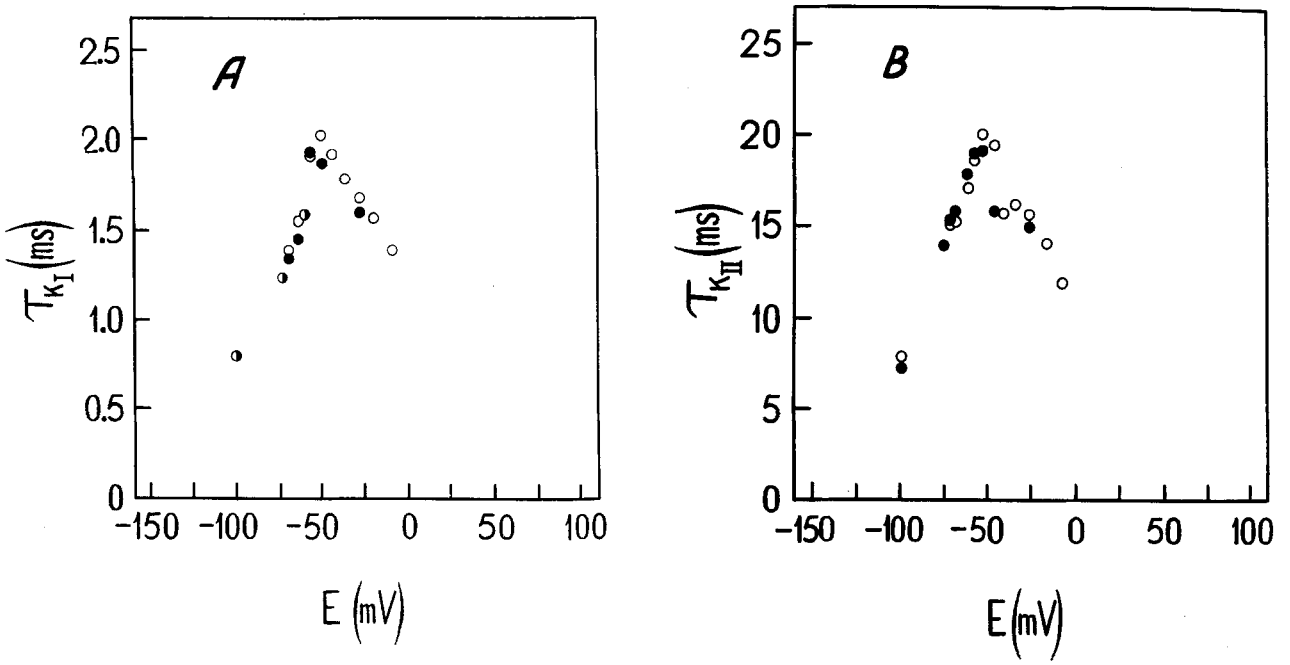

Fig. 8. The relationships $\tau_{K_I}-E$ (*A*) and $\tau_{K_{II}}-E$ (*B*) measured with prepulses E_1 of two different durations. The amplitude of E_1 was +67 mV; the duration of E_1 was 50 msec (open circles) and 500 msec (filled circles). The values of *E* on the abscissa are values of the test potential E_2 used. The experiment is the same as in Figs. 6 and 7

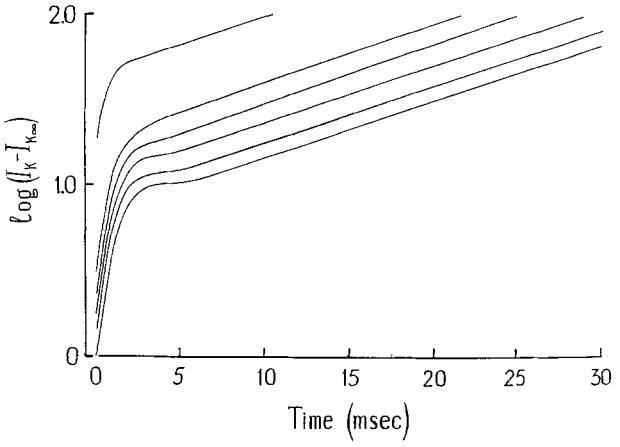

Fig. 9. The Cole-Moore test for repolarization in a Type II fiber. E_1 (in the downward direction) were −62, −42, −32, −3, +8 and +53 mV. E_2 was −104 mV. The instantaneous amplitude of the maximum current (associated with a step from $E_1 = +53$ mV) is normalized to 1. All the other details are as in Fig. 1. Note that the I_K tails associated with E_1 equal to −62 and −42 mV behave as those in Fig. 1 while the I_K tails associated with E_1 equal to −32, −3, +8 and +53 mV have a shoulder lengthening with E_1. Node 372

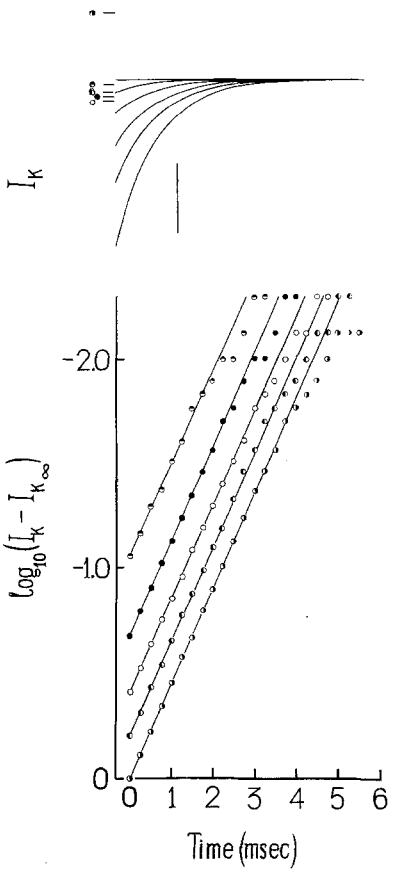

Fig. 10. The Cole-Moore test for repolarization in a Type III fiber. *Above:* I_K tails associated with steps from E_1 (downwards from the base-line): −60, −48, −35, −14, and +60 mV to $E_2 = -98$ mV. I_K levels immediately before a step at these E_1 values are indicated by symbols ◒, ●, ○, ◐, ◑, respectively. Duration of E_1, 50 msec. Note that the I_K tails are parallel which is better seen from graphical analysis below. *Below:* graphical analysis of the I_K tails above. All the details as in Fig. 1. For time constants, *see* Table 2, column 2. For relative values of amplitudes of instantaneous currents on the linear scale, *see* Fig. 5*A*. Node 518

−42 mV have the fast and slow components of the same type as in the bottom graphs of Figs. 1 and 4. However, as E_1 is shifted towards more positive values there appears a delay in the decay of the slow component, which increases with E_1. The fast component (when separated) was in all respects identical to that in the bottom graphs of Figs. 1 and 4 (not shown); after subtraction of the fast component, the delay in the decline of the slow component was much more pronounced (not shown).

It should be noted that after the delay the slow components declines with the same $\tau_{K_{II}}$ for all E_1 as in Type I fibers. The delay thus appears to be an additional process, which develops or becomes apparent at larger prepulses E_1. The delays are not observed at less negative test pulses. In this experiment the next to −104 mV value of E_2 was −83 mV, and the components I_{K_I} and $I_{K_{II}}$ of I_K tails associated with different E_1 and $E_2 = -83$ mV were in all respects like those in Figs. 1 and 4. These fibers thus behave in accordance with the HH formalism only in a certain range of E_1 and E_2.

1.3. Type III fibers. The behavior of these relatively rare fibers is exemplified in Fig. 10. I_K tails decay exponentially (the top), and $I_K - t$ curves shift in parallel along the t-axis as prepulse amplitude is changed (the bottom), in full accordance with Eqs. (7–8). For 12 different E_1 ranged from 60 to −60 mV (here E_2 was −98 mV), τ_K was 0.995 ± 0.015 msec (mean ± SD, $n = 12$, see column 2 in Table 2). At $E_2 \sim -100$ mV the rate of decay of the I_K tail of this node was the same as that of the I_{K_I} current in Type I fibers. The $g_{K_\infty} - E$ relationship here (half-filled circles in Fig. 5*A*) was also the same as $g_{K_{I\infty}} - E$ relationship in Type I fibres. These facts suggest that I_K of the node of Fig. 10 is an uncomplicated I_{K_I} current, i.e. in Type III fibers the slow current $I_{K_{II}}$ is lacking.

2. K *Currents at Repolarization: Analysis*

Two exponential decay of g_K in Type I (most numerous) fibers and the shapes of the steady-state values and relaxation times as functions of E for both components can be accounted for by the assumption that the node usually comprises two dynamic HH K channels with different kinetics and E dependency. The same refers to linearity of instantaneous current-

voltage characteristics of both components. On the other hand, the dual exponential decay of g_K and practically all the above features, when considered separately, may also be accounted for by a three-state model for the K channel. Such a model was recently elegantly used by Chiu (1977) to describe Na inactivation in the frog nerve: an *S*-shape time course of recovery from and dual exponential development of inactivation. In multiple-state models, however, g_{K_I} and $g_{K_{II}}$ will be coupled and the parameters characterizing them will be interrelated. We shall now show that the interrelation required by the models is not observed in experiment.

Let us consider three-state scheme (10)

$$1 \underset{b_1}{\overset{a_1}{\rightleftharpoons}} 2 \underset{b_2}{\overset{a_2}{\rightleftharpoons}} 3 \qquad (10)$$

$$n_1+n_2+n_3=1$$

where a_i and b_i are E-dependent forward and backward rate constants, respectively, and of the three states only one is conducting. Since on repolarization the system starts from the conducting state, it is convenient to take this state to be state 1, that is $g_K(t) \sim n_1(t)$. Scheme (10) is described by two independent linear differential equations yielding the following general solution for $n_1(t)$

$$n_1(t)=G_{11}\exp(-k_1 t)+G_{12}\exp(-k_2 t)+n_{1\infty} \qquad (11)$$

where k_1 and k_2 are reciprocal relaxation times in every kinetic response obtained as eigenvalues from the characteristic equation, G_{11} and G_{12} are amplitude coefficients of the exponential terms defined from initial conditions and expressed as

$$G_{11}=\frac{(a_1+b_1-k_2)(n_{10}-n_{1\infty})+b_1(n_{30}-n_{3\infty})}{k_2-k_1} \qquad (12)$$

$$G_{12}=\frac{(a_1+b_1-k_1)(n_{10}-n_{1\infty})+b_1(n_{30}-n_{3\infty})}{k_1-k_2} \qquad (13)$$

and

$$n_{1\infty}=b_1 b_2/(a_1 a_2+a_1 b_2+b_1 b_2). \qquad (14)$$

In a repolarization kinetic response all the parameters entering Eq. (11) are experimentally measured quantities: $k_{1,2}=1/\tau_{K_{I,II}}$ or $k_{1,2}=1/\tau_{K_{II,I}}$; $G_{11}=g_{K_{I0}}$, $G_{12}=g_{K_{II0}}$ or vv; $n_1=g_{K_\infty}$ (with $\bar{g}_K$ normalized to 1, which will be assumed throughout the analysis).

The repolarization data obtained for Type I fibers are characterized by three main features. (i) τ_{K_I} and τ_{K_i} are independent of E_1 (Table 2). This is true for any monomolecular reaction because k_1 and k_2 are only defined by a_i and b_i which do not depend on E_1. It is obvious then that independent translation of each g_K component alone cannot be the basis for discrimination between one-channel and two-channel models. The other two features are of greater utility in this respect. They are: (ii) $g_{K_{I0}}$ and $g_{K_{II0}}$ do not depend on E_2; that is, the ratio $g_{K_{I0}}/g_{K_{II0}}$ is constant at all E_2 values (Fig. 7); (iii) τ_{K_I} and $\tau_{K_{II}}$ depend on E_2 in such a way that $\tau_{K_I}-E$ and $\tau_{K_{II}}-E$ relationships when plotted to the same vertical scale (msec) are not parallel (it follows from Figs. 2-3 or Fig. 8*A*, *B*).

Consider feature ii. Figure 6 says that $g_{K_\infty} \to 0$ when E_2 is in the vicinity of -100 mV. The condition $g_{K_\infty}=0$ means that $n_{1\infty}=0$. It can be shown (Makovsky, 1979) that the latter condition imposes constraints on a_i, b_i such that k_1 and k_2 obtained from the characteristic equation and introduced into Eqs. (12)-(13) give either G_{11} or G_{12} tending to zero. Whether this will be the amplitude coefficient of the fast or slow term in Eq. (11) depends on whether the first forward transition in scheme (10) is respectively slow ($a_1<a_2$) or fast ($a_1>a_2$). Thus with sufficiently large and negative E_2, mono-exponential kinetics must be observed. This prediction of three-state model (completely fulfilled for dual-exponential development of the Na channel inactivation in frog nerve (Chiu, 1977)) does not, however, agree with experimental data of Figs. 1 and 4.

Feature iii allows another test of the model. The data of Fig. 7 were obtained with $E_1=67$ mV, that is with $n_{10}=1$ (*see* Fig. 5*A*) and $n_{30}=0$. Again in the vicinity of -100 mV, $n_{1\infty}=0$ and $n_{3\infty}=1$. Then in this E range, one must have

$$\frac{g_{K_{I0}}}{g_{K_{II0}}}=\frac{G_{11}}{G_{12}}=\frac{a_1(E)-k_2(E)}{k_1(E)-a_1(E)}=\text{const}, \qquad (15)$$

and $\tau_{K_I}-E$ and $\tau_{K_{II}}-E$ plots should have then been parallel; they were not.

Thus the three-state mechanism with one conducting state cannot explain the dual-exponential decline of g_K and, as a consequence, the dependence of g_K kinetics on initial conditions.

In general, an x-state scheme yields $(x-1)$ exponentials. If, again, only the first state is conducting, then (as $\bar{g}_K$ is taken to be 1)

$$g_K(t)=n_1(t)=\sum_i^{x-1} G_{1i}\exp(-k_i t)+n_{1\infty}.$$

In applying this formula to our experimental results we should assume that either $(x-3)$ amplitudes are negligibly small or $(x-3)$ values from the set of k_i are much larger than the other two. Besides, with E_1 large and positive (when $g_{K_\infty}=1$) and E_2 large and negative (when $g_{K_\infty}=0$) all n_{i0}, except $n_{10}(=1)$ will be 0 and so will be all $n_{i\infty}$, except $n_{x\infty}(=1)$. Then expressing the ratio $g_{K_{I0}}/g_{K_{II0}}$ through rate constants

a_i and b_i one must obtain an expression similar to Eq. (15). We can thus conclude that multiple-state models with one conducting state are not likely to describe our experimental results.

The linearity of current-voltage characteristics in Fig. 6 suggests the possibility of a process with two conducting states. Let these states, in model (10), be states *1* and *2*. Then

$$g_K(t)=n_1(t)+n_2(t)$$
$$=(G_{11}+G_{21})\exp(-k_1 t)+(G_{12}+G_{22})\exp(-k_2 t)$$
$$+G_\infty$$

where G_{21} and G_{22} are amplitude coefficients relating to state *2*. It can be shown (Makovsky, 1979) that the condition $G_\infty=0$ gives $b_2=0$ in Eq. (14), and this leads to $k_{1,2}=a_{1,2}$ or $k_{1,2}=a_{2,1}$. With E_1 sufficiently large and positive and E_2 sufficiently large and negative, $n_{30}=0$ and $n_{3\infty}=1$. It can also be shown then (Makovsky, 1979) that

$$\frac{g_{K_{I0}}}{g_{K_{II0}}}=\frac{n_{10}}{n_{20}}=\frac{a_2(E)-n_{10}k_2(E)}{n_{10}k_1(E)-a_2(E)}=\text{const.}$$

As $n_{10}\neq 0$, this ratio is always more than zero and less than infinity. This means that dual-exponential decay of g_K can be observed even at extreme negative values E_2 and at any relative values of conductances in states *1* and *2*, but the predicted $\tau_{K_I}-E$ and $\tau_{K_{II}}-E$ plots (which proves to be parallel again) do not agree with experiment. Of course, in a model with two conducting states no less than four states are needed to account for depolarization delay of g_K turn on kinetics. But we do not believe these models to be likely either, for the same reasons as discussed above for multiple-state models with one conducting state.

The failure of multiple-state models to account for dual-exponential decay of g_K in the present experiments is evident. As was noted above, in these models g_{K_I} and $g_{K_{II}}$ are coupled and the parameters characterizing them are interrelated. In our experiments, however, no coupling was observed.

3. K *Currents at Depolarization: Results*

3.1. Type I Fibers. Fig. 11 shows I_K-t curves associated with depolarizing steps, under the Cole-Moore conditions, for a fiber belonging to Type I according to classification given in section 1.1. In this experiment the node was in high K solution 4. Altogether there were 12 different prepulses E_1 and the same test pulse E_2. The curves obtained are spaced 0.25 msec apart for clarity. It can be seen that, in accordance with Eqs. (5)-(6), the curves shift to the right along the t-axis with more negative E_1 but the shifts are non-parallel: the more negative is E_1, the more slowly curves rise. I_K-t curves of this type were observed with all E_2 applied (between about $-30\div 60$ mV in 2.5 mM KCl and $10\div 60$ mV in 128mM KCl). Similar results have also been reported by others for *R. esculenta* (Palti et al., 1976).

It might be assumed (although not easily explained) that this dependence of I_K kinetics on initial conditions is due to E_1 dependence of the HH time constant τ_n. Had this been so, the I_K-t curves of Fig. 11 plotted as $\ln(1-I_K^{1/x})$ against t (with I_{K_∞} taken to be 1) should have been straight, if not parallel, lines, if the value of x were properly adjusted (this follows from Eqs. (3)-(4), if $E_K=\text{const}$ which was shown above to be really the case). No such value of x could be found, which means that I_K kinetics in this case cannot be presented by n^x formalism at all. The same conclusion has also been drawn by Palti et al. (1976) for analogous I_K-t curves with *R. esculenta*.

3.2. Type II Fibers. On depolarization, I_K kinetics in these fibers were practically indistinguishable from those of Type I fibers. This result is consistent with the fact that the difference between the two types of fibers could be detected only with sufficiently negative test potentials (section 1.2).

3.3. Type III Fibers. In fibers of this type under the same experimental conditions as in Fig. 11 I_K-t curves shift in parallel; i.e., the Cole-Moore translation of g_K is observed directly. Analogous results were obtained with different E_2 (23, 42, and 60 mV) (not shown).

The I_K-t curves associated with the same E_1 (-98 mV) and various E_2 (ranged from -60 to 60 mV) could be made to superimpose by double translation along coordinates $\log I_K$ and $\log t$ (Makovsky, 1979), which means that in Type III fibers I_K kinetics can be described by the n^x formalism (Dodge 1963; Hille 1967*a*). Figure 12 presents five of these I_K curves plotted as $\ln(1-I_K^{1/x})$ against t (from the same node as in Fig. 10). One can clearly see that plots are linear with all E_2 used and with $x=4$ only. With smaller x (2) the curves displayed, at small t, a positive curvature and with greater t (5 or 6) a negative curvature (not shown). The same value of $x=4$ was found with all other E_2 (-60, -40, -20, 50 mV) and with different E_1 (-60, -32 mV); that means $x=4$ is the correct value of x in Eq. (4).

4. K *Currents at Depolarization: Analysis*

On depolarization, I_K currents in Type III fibers obey n^4 kinetics and do not require special treatment. It is

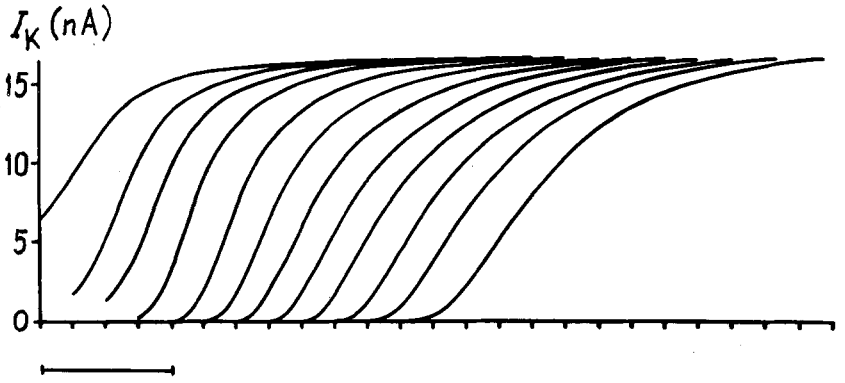

Fig. 11. The Cole-Moore test for depolarization in a Type I fiber. The $I_K - t$ curves are spaced apart at 0.25 msec for clarity. E_1 (running from left to right): −32, −50, −55, −65, −75, −88, −103, −113, −120, −132, −146, and −170 mV. E_2 (10 msec) was +50 mV. (For other details, *see* text.) Note that the $I_K - t$ curves are nonparallel. 128 mM KCl Ringer $+3 \cdot 10^{-4}$ mM TTX. Leakage current was subtracted. Calibration time bar: 1 msec. Node 146

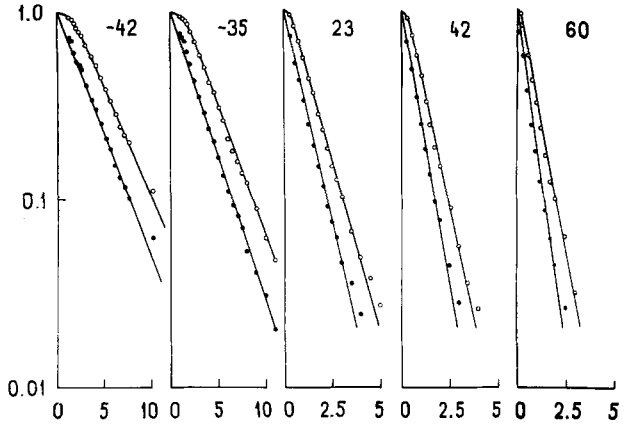

Fig. 12. $I_K - t$ curves of a Type III fiber associated with E steps from E_1 (−98) to 5 E_2 indicated near the curves plotted as $\ln(1 - I_K^{1/x})$ against t. ○ - $x=2$; ● - $x=4$. 128 mM KCl Ringer $+3 \cdot 10^{-4}$ mM TTX. Node 518

sufficient to note that $\tau_n - E$ and $n_\infty - E$ relationships were obtained from $\ln(I_{K\infty}^{1/4} - I_K^{1/4}) - t$ plots (Makovsky, 1979) and proved to be very near to those in *R. pipiens* (Dodge, 1963; Hille, 1967*a*). Again, repolarization data indicate that the fast component I_{K_I} is invariant with respect to the type of a fiber and it is not coupled to the slow component $I_{K_{II}}$. These facts and the mode of action of TEA (Section 5) suggest that I_{K_I} and $I_{K_{II}}$ are due to separate K channels, a fast and a slow.

Depolarization data for Type III fibers further suggest that the fast channel is the familiar n^4 channel of *R. pipiens*. The slow channel, at least in most fibers, is also of the HH type: repolarization data show that it is controlled by a single first-order variable, and its steady-state and kinetic characteristics are like those in HH. In essence, the only unknown parameter for the slow channel remains the value of x.

On the basis of these data we attempted to represent I_K of Type I fibers in Fig. 11 as the sum of two HH currents, I_{K_I} and $I_{K_{II}}$. If, as above, we take I_{K_I} as the fast current, then x_I and ratio $\bar{g}_{K_{II}}/\bar{g}_{K_I}$ could be considered known. However, we did not use them. Instead, we tried to find all the HH parameters with least squares and compare them to observations.

The model analyzed was as follows.

$$I_K = I_{K_I} + I_{K_{II}}$$
$$I_{K_I} = g_{K_I}(E - E_{K_I})$$
$$I_{K_{II}} = g_{K_{II}}(E - E_{K_{II}})$$
$$g_{K_I} = \bar{g}_{K_I} \cdot n_I^{x_I}$$
$$g_{K_{II}} = \bar{g}_{K_{II}} \cdot n_{II}^{x_{II}}.$$

As under the conditions we used $E_{K_I} = E_{K_{II}} = \text{const}$ (Fig. 7), and the above equations yielded:

$$g_K = g_{K_I} + g_{K_{II}}. \tag{16}$$

Further obvious assumptions were that at $E = 50$ mV, $n_{I_\infty} = n_{II_\infty} = 1$: they followed from Fig. 5*A* and *B*. Eq. (16) then acquired the form

$$g_K(t) = \bar{g}_{K_I}\left[1 - (1 - n_{I_\infty}(E_1)) \exp\left(-\frac{t}{\tau_{n_I}}\right)\right]^{x_I} + \bar{g}_{K_{II}}\left[1 - (1 - n_{II_\infty}(E_1)) \exp\left(-\frac{t}{\tau_{n_{II}}}\right)\right]^{x_{II}}. \tag{17}$$

To estimate a possible position of the absolute minimum we first fitted Eq. (17) to individual curves in Fig. 11. The calculated parameters of the curves behaved with E_1 just as predicted by the HH model: x_I and x_{II} (both 4) as well as $\bar{g}_{K_I}$ and $\bar{g}_{K_{II}}$ were constant within a few percent and so practically were τ_{n_I} and $\tau_{n_{II}}$, at least with moderate E_1; n_{I_∞} and n_{II_∞} increased with E_1 (Table 3). The values found were then taken as coordinates of the starting point of the descent in the search of the absolute minimum of variance under the constraint that $\bar{g}_{K_I}$, $\bar{g}_{K_{II}}$ and τ_{n_I}, $\tau_{n_{II}}$ were the same for all 12 curves. The simultaneous fitting yielded $x_I = x_{II} = 4$; $\bar{g}_{K_I} = 0.61$, $\bar{g}_{K_{II}} = 0.39$; $\tau_{n_I} = 0.24$ msec, $\tau_{n_{II}} = 0.69$ msec; n_{I_∞} and n_{II_∞} depended then on E_1 as shown in Fig. 13. With these values the $I_K - t$ curves in Fig. 11 were fitted to line thickness.

Table 3

E_1 (mV)	−32	−50	−55	−65	−75	−88	−103	−113	−120	−132	−146	−170
$\bar{g}_{K_I}$	0.63	0.61	0.61	0.61	0.61	0.61	0.60	0.60	0.61	0.60	0.60	0.60
$\bar{g}_{K_{II}}$	0.37	0.39	0.39	0.39	0.39	0.39	0.40	0.40	0.39	0.40	0.40	0.40
n_{I_∞}	0.48	0.17	0.01	0.07	0.02	0.05	0.03	0.02	0.00	0.00	0.00	0.00
n_{II_∞}	1.00	0.83	0.81	0.60	0.43	0.31	0.20	0.11	0.08	0.03	0.00	0.00
τ_{n_I} (msec)	0.32	0.26	0.24	0.23	0.24	0.25	0.25	0.27	0.33	0.35	0.44	0.45
$\tau_{n_{II}}$ (msec)	0.62	0.62	0.62	0.62	0.64	0.65	0.70	0.73	0.75	0.80	0.81	0.81

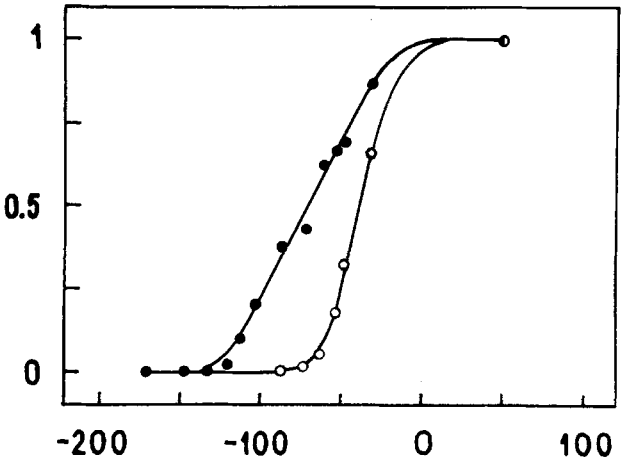

Fig. 13. $n_{I_\infty} - E$ (open circles) and $n_{II_\infty} - E$ (filled circles) relationships obtained from fitting Eq. (18). E values from −170 to −32 mV are the E_1 values shown in Fig. 11; $E = +50$ mV is E_2 in Fig. 11. (For details of computation, *see* text)

One can easily see that the predictions of the modified HH model are fully consistent with the data measurable in direct experiment: the fast component g_{K_I} makes a larger contribution to g_K, is activated by a somewhat more positive E range and depends more strongly on E as compared with the slow component $g_{K_{II}}$ (repolarization data of Fig. 5), and x_I has the correct value of 4. It is therefore very likely that the slow channel kinetics can also be described as n^4.

In the present study initial depolarization conditions were changed by varying the prepulse amplitude. Somewhat more complicated results have been obtained by Ganot et al. (1978) with varying prepulse duration. Our unpublished calculations, analogous to those described above, show that the model proposed could account for most of their results; furthermore, $x_I = x_{II} = 4$ were found to give the best fit.

5. *The Mode of Action of TEA*

The detailed report of these experiments will be published elsewhere, and now we will only summarize data relevant to the results of the kinetic analysis presented above.

In Type III fibers TEA failed to affect the g_K kinetics either at depolarization or repolarization, and its action, including the dose-effect curve, was the same as that reported by Hille (1967*a*, *b*) for *R. pipiens*.

Type II fibers were not encountered in these experiments. In Type I fibers, on repolarization, TEA did not change τ_{K_I} and $\tau_{K_{II}}$ but appreciably increased the ratio $\bar{g}_{K_{II}}/\bar{g}_{K_I}$, suggesting that the fast component g_{K_I} was several times more sensitive to TEA than the slow component $g_{K_{II}}$. On depolarization, TEA lengthened the rate of rise of $I_K - t$ curves in these fibers in much the same way reported by Koppenhöfer (1967) for *X. laevis*. Estimates showed that this lengthening could be accounted for by smaller contribution of the fast component to the overall I_K in the presence of TEA. The data of the pharmacological analysis are thus in full agreement with those obtained in the kinetic analysis.

Discussion

The results obtained in the present study can be summarized as follows. In contrast to *R. pipiens*, in most *R. ridibunda* nerve fibers there is an additional, slow K current component uncoupled to the fast component n^4 (termed here n_I^4 component). The turning on of this slow component can also be described by n^4 kinetics (and this component is termed n_{II}^4), although on repolarization its turn-off kinetics sometimes reveal an additional process preceding the exponential decline. It is this slow component that brings about the nontranslational behavior of I_K. The component was attributed to a slow K channel while the fast K channel appears to be the same as in *R. pipiens*. The action of TEA is fully consistent with this two-K-channel picture, the slow channel being less sensitive to TEA than the fast channel.

Although differential action of TEA on the fast and slow K currents provides further strong evidence

for two different K channels, it would be interesting to find a representation which could cover the results obtained within a one-K-channel model.

We tried some models but without success. Besides multiple-state models considered briefly in section 2, depolarization data taken separately might be accounted for by many models. Among them the most simple are those based on modification of the original HH model, such as supplementation of the n^4 kinetics by some additional process or introduction of cooperative interaction between the HH n-subunits. Repolarization data, however, indicate that these modifications are unlikely condidates. In the first model we could not obtain constant ratio $g_{K_{I0}}/g_{K_{II0}}$ with different repolarizing test potentials, as in Fig. 7, and in the second model, according to calculations of Hill and Chen (1971*a*), g_K "decreases, typically in a repolarization, following a more or less first-order curve."

The ability of the HH formulation to describe novel results is very impressive, but there are two points concerning the present experiments in which the model is inadequate. First, and most important, the appearance, at extreme initial and final potentials, of a delay preceding exponential decline of the slow K current on repolarization, in Type II fibers indicates that the HH kinetics are only a special case of some kinetics of a more general type. As depolarization data are not easy to use to reveal and assess possible kinetic difference between g_{K_I} and $g_{K_{II}}$ in Type I and Type II fibers, we did not attempt to construct a general model, but we consider it an important matter. All that we can say now is that a three-state model for a slow K channel with $k_1=k_2=k$, giving $(G_{11}+tG_{12})\exp(-kt)+n_{1\infty}$ as the general solution to scheme (10), with a delay when t is small and exponential decay when t is large, does not account for the observed E-dependence of the delay. The other point is dependence of τ_{n_I} and $\tau_{n_{II}}$ on extreme initial hyperpolarizing potentials (Table 3). Its lengthening with more negative E_1 is not the result of separate processing of the curves, and it is not likely that it was due to a damaging effect of large hyperpolarization. Though this effect may be considered unimportant for usual experimental situations, it is interesting because in squid such dependence was not observed (Cole & Moore, 1960). It would be of interest to check the possibility of whether such an effect might be produced by some interaction imposed on n-subunits by strong initial hyperpolarization.

Having postulated that, in general, a K channel either fast or slow obeys n^x formalism, i.e., it displays the properties of translation and induction, one can infer, following theoretical analysis of Hill and Chen (1971*a*, *b*), that cooperative interaction either of gating subunits within a channel or between the channels cannot be the basis for such kinetics; experimental data of Sigworth (1979) seem to agree with this conclusion. Aggregation models, at least simple ones, are not likely either (Hill & Chen, 1971*b*). As g_K-t curves cannot be used to distinguish between the classical HH model ($k=0$) and k-models of Hill and Chen (1972; Chen, 1976), both single-conductance (HH) and multiple-conductance (Hill & Chen) mechanisms are possible for fast and slow K channels.

The coupling between the K channels and Na channels (Mullins, 1968) is strongly excluded because Hoyt (1971) has shown that the property of translation (displayed by the K current) and inactivation (displayed by the Na current) cannot be coupled. For this same reason the activation and inactivation properties within the fast K channel observed in the present work must be uncoupled, too. As to the difference between the fast and slow K channels it might be due mostly to different heights of the activation energies and/or the effective charge of gating subunits. It can be noted that an EIM channel has very different relaxation times in different lipid bilayers (Bean, 1973).

The role of fast and slow K channels with the properties we have measured was studied in the repetitiveness of amphibian sensory fibers (Makovsky, 1979). Spike trains were computed on the basis of the Dodge-HH model (Hille, 1967*a*) modified to cover the $g_{K_{II}}$ component. The results obtained (Krylov & Makovsky, 1978, 1979) show that the K channels are important for analog-code input-output transformation of a signal. The fast channels appear to be mostly responsible for the output frequency as a logarithmic function of constant current strength (Bromm & Frankenhaeuser, 1972). The slow channels ensure spike frequency adaptation (increase in time of interspike intervals during the action of a maintained stimulus) and numeric coding (increase in number of spikes in a discharge with stimulus strength). Spike frequency adaptation has previously been shown to be due to a slow K channel in molluscan neurones (Partridge & Stevens, 1976). Although both types of aperiodic processes in amphibian sensory fibers experimentally are well known (Erlanger & Blair, 1938; Dodge, 1963; Vallbo, 1964*a*, *b*; Honerjäger, 1968; Bergman, 1969; *see also* literature in Stämpfli & Hille, 1976), they failed to be described in terms of the HH model for the node (Dodge, 1963; Frankenhaeuser & Vallbo, 1965). By contrast, consideration of the slow K channel not only accounts for these processes as such but also for their variability in different amphibian fibers (well known by experimentors and studied by Vallbo, 1964*a*), when variability

in the properties of slow K channels as described in the present study are taken into account. As the coding properties of fibers for different senses must differ, the variability of the density of the slow K channels must be of physiological value. It is interesting to note that previously the role of the dynamic K channels has been considered unknown because they do not practically participate in repolarization of the excited membrane of the node (Dodge, 1963; Frankenhaeuser & Huxley, 1964; Khodorov, 1975).

To summarize, we conclude that in *R. ridibunda* node the departure of the g_K behavior from the HH kinetics is due to the involvement of a slow K channel. The same may be true for other amphibia where the Cole-Moore effect is not observed (Makovsky, 1975; Palti et al., 1976; Ganot et al., 1978). In *R. pipiens* both the Cole-Moore and other tests (Dodge, 1963; Hille, 1967*a*) give no indication of such channels. However, here spike frequency adaptation is also observed (Dodge, 1963). A possible source for this adaptation might be slow Na inactivation described by Chiu (1977), but clear-cut increase in the undershoot amplitudes with time makes one suspect the involvement of a slow K system. If $E_{K_{II}}$ of this system would be as large as the resting potential which amounts to −81 mV (Campbell & Hille, 1976), then under certain conditions $g_{K_{II}}$ as small as only 10% of g_{K_I} could produce pronounced adaptation. We feel therefore that it is worthwhile to look for a slow K system in *R. pipiens* node under voltage clamp conditions. Either result might be useful in interpretation of I_K noise measurements (*cf.* Begenisich & Stevens, 1975; Chen, 1976).

The authors would like to thank Prof. C.F. Stevens for interest in the work, encouragement, and helpful discussion of the results; Prof. R. Stämpfli for advice and many helpful discussion of some of the results; Dr. G.N. Mozhaeva and Dr. A.P. Naumov for interest in the work and discussions of the results.

References

Adam, G. 1973. The effect of potassium diffusion through the Schwann cell layer on potassium conductance of the squid axon. *J. Membrane Biol.* **13**:353

Adelman, W.J., Jr., Palti, Y., Senft, J.P. 1973. Potassium ion accumulation in a periaxonal space and its effect on the measurement of membrane potassium ion conductance. *J. Membrane Biol.* **13**:387

Bean, R.S. 1973. Protein-mediated mechanisms of variable ion conductance in thin lipid membranes. *In:* Membranes - A Series of Advances. G. Eisenman, editor. Vol. 2, pp. 409-477. Lipid Bilayers and Antibiotics. Marcel Dekker, New York

Begenisich, T., Stevens, C.F. 1975. How many conductance states do potassium channels have? *Biophys. J.* **15**:843

Bergman, C. 1969. Seuil d'excitation et regimes d'activité du noeud de Ranvier. Thèse doctorate. Paris

Brent, R.P. 1973. Algorithms for minimization without derivatives. Prentice-Hall, Englewood Cliffs, N.J.

Bromm, B., Frankenhaeuser, B. 1972. Repetitive discharges of the excitable membrane computed on the basis of voltage clamp data. *Pfluegers Arch.* **332**:21

Campbell, R.T., Hille, B. 1976. Kinetic and pharmacological properties of the sodium channel of frog skeletal muscle. *J. Gen. Physiol.* **67**:309

Chen, Y. 1976. Differentiation of channel models by noise analysis. *Biophys. J.* **16**:965

Chiu, S.Y. 1977. Inactivation of sodium channels: Second order kinetics in myelinated nerve. *J. Physiol. (London)* **273**:573

Cole, K.S., Moore, J. 1960. Potassium ion current in the squid giant axon: Dynamic characteristic. *Biophys. J.* **1**:1

Dodge, F.A. 1963. A study of ionic permeability changes underlying excitation in myelinated nerve fibers of the frog. Ph.D. Thesis. The Rockefeller Institute, New York

Dubois, J.M., Bergman, C. 1975. Potassium accumulation in the perinodal space of frog myelinated axons. *Pfluegers Arch.* **358**:111

Erlanger, J., Blair, E.A. 1938. Comparative observations on motor and sensory fibres with special reference to repetitousness. *Am. J. Physiol.* **212**:431

Frankenhaeuser, B. 1962. Instantaneous potassium currents in myelinated nerve fibres of *Xenopus laevis*. *J. Physiol. (London)* **160**:46

Frankenhaeuser, B. 1963. A quantitative description of potassium currents in myelinated nerve fibres of *Xenopus laevis*. *J. Physiol. (London)* **169**:424

Frankenhaeuser, B., Huxley, A.F. 1964. The action potential in the myelinated nerve fibre of *Xenopus laevis* as computed on the basis of voltage clamp data. *J. Physiol. (London)* **171**:302

Frankenhaeuser, B., Vallbo, A.B. 1965. Accommodation in myelinated nerve fibres of *Xenopus laevis* as computed on the basis of voltage clamp data. *Acta Physiol. Scand.* **63**:1

Ganot, G., Palti, Y., Stämpfli, R. 1978. Cole-Moore effect in the frog nerve. *Proc. Nat. Acad. Sci. USA* **75**:3254

Hill, T.L., Chen, Y. 1971*a*. On the theory of ion transport across the nerve membrane. II. Potassium ion kinetics and cooperativity (with $x=4$). *Proc. Nat. Acad. Sci. USA* **68**:1711

Hill, T.L., Chen, Y. 1971*b*. On the theory of ion transport across the nerve membrane. III. Potassium ion kinetics and cooperativity (with $x=4, 6, 8$). *Proc. Nat. Acad. Sci. USA* **68**:2488

Hill, T.L., Chen, Y. 1972. On the theory of ion transport across the nerve membrane. IV. Noise from the open-close kinetics of K^+ channels. *Biophys. J.* **12**:948

Hille, B. 1967*a*. A pharmacological analysis of the ionic channels of nerve. Ph.D. Thesis. The Rockefeller University, New York

Hille, B. 1967*b*. The selective inhibition of delayed potassium currents in nerve by tetraethylammonium ion. *J. Gen. Physiol.* **50**:1287

Hodgkin, A.L., Huxley, A.F. 1952. A quantitative description of membrane current and its application to conductance and excitation in nerve. *J. Physiol. (London)* **117**:500

Honerjäger, P. 1968. Die repetitive Aktivität motorischer und sensibler markhaltiger Nervenfasern des Frosches. *Pfluegers Arch.* **303**:55

Hoyt, R.C. 1971. Independence of the sodium and potassium conductance channels. A kinetic argument. *Biophys. J.* **11**:110

Ilyin, V.I., Katina, I.E., Lonskii, A.V., Makovsky, V.S., Polishchuk, E.V. 1973. Components of potassium current in the node of Ranvier under voltage clamp conditions. *In:* Membrane Biophysics. D.P. Zablotskaite, E.V. Narushevichus, and A.P. Skersys, editors. P. 286. Kaunas Institute of Medicine, Kaunas (*in Russian*)

Ilyin, V.I., Katina, I.E., Lonskii, A.V., Makovsky, V.S., Polishchuk, E.V. 1974*a*. The FitzHugh-Cole-Moore effect in the nodal membrane. *In:* Functional Morphology, Genetics and Biochemistry of the Cell. A.S. Troshin, editor. P. 239 Nauka, Leningrad *(in Russian)*

Ilyin, V.I., Katina, I.E., Lonskii, A.V., Makovsky, V.S., Polishchuck, E.V. 1974*b*. Activation potential ranges of potassium conductance components of the nodal membrane in the frog *Rana ridibunda*. *In:* Functional Morphology, Genetics and Biochemistry of the Cell. A.S. Troshin, editor. P. 242. Nauka, Leningrad *(in Russian)*

Ilyin, V.I., Katina, I.E., Lonskii, A.V., Makovsky, V.S., Polishchuk, E.V. 1977. Evidence for two independent components of potassium current in the nodal membrane of the frog *Rana ridibunda*. *Dokl. Acad. Nauk SSSR* **234**:1467 *(in Russian)*

Khodorov, B.I. 1975. General physiology of excitable membranes. Nauka, Moscow *(in Russian)*

Koppenhöfer, E. 1967. Die Wirkung von tetraäthylammoniumchlorid auf die Membranströme Ranvierscher Schnurringe von *Xenopus laevis*. *Pfluegers Arch.* **293**:34

Krylov, B.V., Makovsky, V.S. 1978. Spike frequency adaptation in amphibian sensory fibres is probably due to slow K channels. *Nature (London)* **275**:549

Krylov, B.V., Makovsky, V.S. 1979. Ionic mechanism for analog-code transformation in nerve fibre membrane. *Dokl. Akad. Nauk SSSR* **244**:220

Lonskii, A.V., Ilyin, V.I., Malov, A.M. 1972. An improved voltage clamp method for the node of Ranvier. *Physiol. J. SSSR* **58**:136 *(in Russian)*

Makovsky, V.S. 1975. Comments on the time-dependence of the potassium permeability rate constants in the nodal membrane. *Tsitologiya* **17**:55 *(in Russian)*

Makovsky, V.S. 1979. Potassium channels of the Ranvier node membrane and their role in electric activity of myelinated nerve fibres. Ph.D. Thesis. Leningrad Nuclear Physics Institute, Gatchina, Leningrad District

Mullins, L.J. 1968. A single or a dual channel mechanism for nerve excitation. *J. Gen. Physiol.* **52**:550

Nonner, W. 1969. A new voltage clamp method for Ranvier node. *Pfluegers Arch.* **309**:176

Palti, Y., Ganot, G., Stämpfli, R. 1976. Effect of conditioning potential on potassium current kinetics in the frog nerve. *Biophys. J.* **16**:261

Partridge, L.D., Stevens, C.F. 1976. A mechanism for spike frequency adaptation. *J. Physiol. (London)* **256**:315

Schwarz, J.R., Vogel, W. 1971. Potassium inactivation in single myelinated nerve fibres of *Xenopus laevis*. *Pfluegers Arch.* **330**:61

Sigworth, F. 1979. The Cole-Moore delay: Cooperativity among potassium channels? *Biophys. J.* **25**:196*a*

Stämpfli, R., Hille, B. 1976. Electrophysiology of the peripheral myelinated nerve. *In:* Frog Neurobiology. R. Llinas and W. Precht, editors., pp. 1–32. Springer-Verlag, Berlin – Heidelberg

Vallbo, A.B. 1964*a*. Accommodation of single myelinated nerve fibres from *Xenopus laevis* related to the type of end organ. *Acta Physiol. Scand.* **61**:413

Vallbo, A.B. 1964*b*. Accommodation related to inactivation of the sodium permeability in single myelinated nerve fibres from *Xenopus laevis*. *Acta Physiol. Scand.* **61**:429

Received 3 July 1980

Note in Proof

This paper was published posthumously after the untimely death of V.S. Makovsky.